Sustainable Energy Technologies and Assessments 60 (2023) 103552

Contents lists available at ScienceDirect

Sustainable Energy Technologies and Assessments

journal homepage: www.elsevier.com/locate/seta

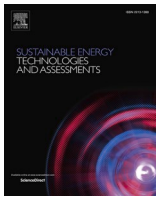

Research on X-ray-based energy conversion technology and assessment of application prospect

Yishui Wu [a], Zhiheng Xu [a,b,*], Yunpeng Liu [a,b], Tongxin Jiang [c], Haisheng San [c], Xiaobin Tang [a,b,*]

[a] Department of Nuclear Science and Technology, Nanjing University of Aeronautics and Astronautics, Nanjing 211106, China
[b] Key Laboratory of Nuclear Technology Application and Radiation Protection in Astronautics, Ministry of Industry and Information Technology, Nanjing 211106, China
[c] Pen-Tung Sah Institute of Micro-Nano Science and Technology, Xiamen University, Xiamen 361005, China

ARTICLE INFO

Keywords:
X-ray
Energy conversion
Radiation monitoring
Radio-voltaic
Radio-luminescent

ABSTRACT

A new type of wireless energy transfer (radiation energy to electricity) power system is proposed for small-scale distributed energy utilization. To utilize radiation energy efficiently, energy conversion technologies based on different conversion modules and dissimilar material combination schemes are used. A variety of schemes such as single photovoltaic cell and single/multilayer fluorescent layer integrated with photovoltaic cell are designed. The maximum power density ranges from 7.93 nW/cm^3 (tube voltage: 30 kV, tube current: 1 mA) to 6.7 μW/cm^3 (tube voltage: 110 kV, tube current: 1 mA). After the structure layout of the system is matched and optimized, the maximum output power in radio-luminescent mode can be much higher than that in radio-voltaic mode. In particular, the maximum output power of conversion modules with a stacked layer can be increased by more than 36 times in radio-luminescent mode compared to radio-voltaic mode. At the same time, the effect of the distance of wireless energy transfer on the output performance of the energy conversion module is analyzed. To adjust the radiation intensity and field parameters better, X-ray tube is used as the radiation excitation source for performance testing and analysis. The performance attenuation of different energy conversion modules is similar when responding to X-ray over long distances. Compared with the radio-voltaic mode, the findings of this paper show that the output power of the system based on the radio-luminescent mode can be an order of magnitude higher.

Introduction

The environment we live in is full of various kinds of energy, such as solar energy, chemical energy, mechanical energy, deformation energy, biological energy, wind energy, heat energy, radiation energy, and many others [1–4]. We can make full use of energy conversion technology, for example, to transport energy over long distances and then convert it into electricity to power electronic devices, to realize wireless self-powered or self-driven power supply/detection/monitoring systems [5–8]. With the rapid development of the space industry, the pace of human exploration is going further, and the new power supply technology along with it is becoming a challenging problem [9]. At present, most space equipment is powered by external solar panels, which depend on light, or built-in chemical cells, which are usually limited in capacity and uneconomic to maintain [10,11]. Radiation energy is almost ubiquitous in these situations and is often difficult to perceive. How to utilize it and at the same time monitor its intensity is a key issue that needs to be addressed.

Through the interaction between the energy conversion device and radioactive particles [12–14], its radiation energy is absorbed and converted into electrical energy, which can directly supply power to micro low-power electronic devices. It not only enables effective monitoring and feedback of the radiation field but also eliminates the need for a dedicated battery to power the device, thus reducing the cost, weight, and potential riskiness of the device in service. This power generation method can obtain energy from the radiation field in the environment and is suitable for the demand of long-life, maintenance-free, and self-powered systems under special conditions. As mentioned at the beginning of this paragraph, its potential application in energy engineering is manifested by harvesting radiant energy and powering low-power devices such as MEMS in space missions. There is also great potential for applications in radiation environment monitoring,

* Corresponding authors at: Department of Nuclear Science and Technology, Nanjing University of Aeronautics and Astronautics, Nanjing 211106, China.
E-mail addresses: xuzhiheng@nuaa.edu.cn (Z. Xu), tangxiaobin@nuaa.edu.cn (X. Tang).

https://doi.org/10.1016/j.seta.2023.103552
Received 18 July 2023; Received in revised form 30 October 2023; Accepted 10 November 2023

intelligent communication, national defense and military [15,16], Internet of Things [17,18], and wireless sensor networks [19].

X-rays are a form of high-energy electromagnetic radiation [20,21], which is one of the common and widely used types of radiation [22–24]. A thorough understanding of the interaction between X-rays and matter has stimulated our motivation to further explore and expand the potential applications of X-ray radiation fields and to explore the feasibility of using them for power generation. Two main modes of transduction were used to convert the radiant energy of X-rays into electricity: the radio-voltaic (RV) mode and the radio-luminescent (RL) mode. In the RV mode, radiation was directly absorbed by the photovoltaic cell and converted into electricity. In the RL mode, radiation was firstly converted into photons in a specific wavelength by the fluorescent material and then converted into electricity by the photovoltaic effect. Most of the current research is focused on transducer materials, device structure optimization, and performance stability. Some research teams are devoted to the preparation of fluorescent materials with excellent luminescence properties and high-quantum-efficiency photovoltaic cells. Xu et al. prepared $CsPbBr_3$ quantum dot films, whose peak emission was well suited with the peak spectral responsivity of GaAs photovoltaic cell. The output power was increased by 28.3 % compared with direct conversion under suitable film parameters [25]. Likemindedly, Li et al. prepared $Cs_3Cu_2I_5$:Mn scintillators with high thermal stability and irradiation hardness, and the output power was increased by 237 % compared with direct conversion [26]. By contrast, photovoltaic cells with suitable quantum efficiency were selected. Zhao et al. optimized the bandgap of the photovoltaic cell to match GAGG:Ce scintillators, resulting in a 10-fold increase in conversion efficiency [27]. The feasibility of converting the radiant energy of X-rays into electricity is well illustrated, including our earlier work, and also indicates the ways to improve the electrical energy output performance. Among them, achieving a good match of each component, including an efficient response between the radioluminescence spectra of the fluorescent material and the quantum efficiency of the photovoltaic cell, is the key to improving the output.

However, the above-mentioned works mainly explored the value of X-rays for power supply, and the variation of electrical parameters representing the output performance with the intensity of the radiation field were not adequately studied. On this basis, this work dissects in detail the variation rules of electrical parameters with radiation field intensity, proposes a new performance optimization scheme, and assesses the prospects for other applications. Considering the huge application potential of wireless energy transfer and the advantages of the radiation energy conversion technology, it is meaningful to carry out the research on the response law of radiation conversion materials to rays and the design of the energy conversion module combination.

In this work, X-ray generators with different energy conversion modes and different combinations of fluorescent materials were designed to meet the demand for different levels of output power within a certain range. The effects of factors such as short-circuit current (I_{sc}), open-circuit voltage (V_{oc}), maximum output power (P_{max}), and power decay rate were investigated. The potential for other applications such as radiation intensity monitoring and wireless energy transfer was further exploited. The results provide a design basis for the development of devices that combine the dual functions of radiation energy conversion and radiation monitoring without relying on an external power source.

Materials and methods

Energy conversion materials

Photovoltaic cell

To adapt to X-ray transduction better, the structural parameters of the GaAs and AlGaInP-based photovoltaic cells are specially designed and fabricated. Structure details are shown in Fig. S1. The effective area of the two photovoltaic cells is approximately 1×1 cm^2, and the overall thickness of the photovoltaic cells is minimized to less than 1 mm. As shown in Fig. 1, the quantum response wavelength range of GaAs is wider than that of AlGaInP. This can be an explanation for the difference in bandgap and radiation conversion capabilities between GaAs and AlGaInP.

Fluorescent material

CsI scintillator and ZnS:Cu fluorescent layer were selected as the two representative radioluminescent materials. The ZnS:Cu fluorescent layer was made by uniformly coating ZnS:Cu phosphors on a highly transparent and flexible substrate with a thickness of just 0.11 mm. The CsI scintillator is 1 cm in thickness and has four faces coated with a reflective layer.

Fig. 1 also shows the peak wavelengths of the radioluminescence spectra of both CsI and ZnS:Cu lie in the range where the quantum efficiency is high, satisfying the matching requirement. The excellent optical properties of CsI and ZnS:Cu such as high light yield and high luminescence intensity have been demonstrated in imaging, radiation detection, and illumination displays [28,29]. This is equally attractive for energy conversion in RL mode. Our previous works showed that ZnS:Cu is a class of fluorescent materials with good luminescence and anti-radiation properties [30–32]. While the transmittance of the two materials corresponding to the peak wavelength of the emission spectra differs considerably, as shown in the green area of Fig. S2.

Experimental conditions and test methods

Optical properties test

The RL spectra were measured by a Cary Eclipse fluorescence spectrophotometer (Agilent Technologies, G9800a) using the X-ray tube to irradiate the ZnS:Cu fluorescent layer and CsI scintillator located in the sample compartment. The emission spectra were recorded for 300–800 nm. The slit width of the emission monochromator was set to 20 nm and the tube voltage of photomultiplier was set to 800 V. The transmittance spectra were measured by UV-visible spectrophotometer (Aucy, UV1901PC). The transmittance spectra were recorded for 300–800 nm. EQE curves were measured by QE-R (Enli Tech).

Electrical performance test

An X-ray tube (SC-T160/1.2–80, Beijing Research Institute of Mechanical & Electrical Technology) was used to generate the radiation

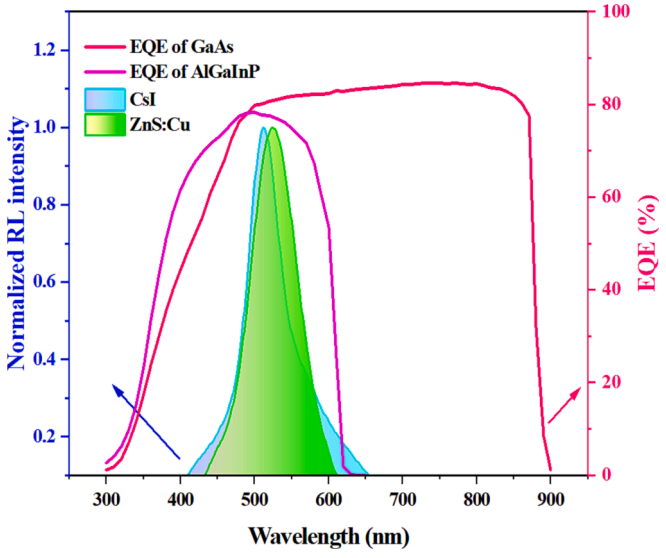

Fig. 1. Radioluminescence spectra of ZnS:Cu fluorescent layer and CsI scintillator, EQE curves of GaAs and AlGaInP.

field. The maximum tube voltage is 160 kV, and the maximum tube current is 1.2 mA. The tube voltage was set at 30, 50, 70, 90, and 110 kV, and the tube current was fixed at 1 mA. In the long-distance test, the photovoltaic cells and the fluorescent materials were fixed within the range of the radiation field on the lead plate, and the distance between the lead plate and the exit of the tube was continuously increased from 10 to 90 cm. *I-V* curves were measured using a dual-channel source meter (Keithley, Model 2636A) after the tube voltage and tube current stabilized. *I-V* curves under the same radiation field intensity condition were measured at least three times to ensure the accuracy of the data. All tests were carried out in a dark radiation-shielded lead room under standard atmospheric pressure and room temperature.

Results and discussion

Radio-voltaic mode analysis

GaAs and AlGaInP photovoltaic cells were placed directly at the X-ray tube exit, and the electrical output was tested at different tube powers. The measured *I-V* curves are shown in Fig. 2. The *I-V* curve consists of a series of points with voltage as the horizontal coordinate and current as the vertical coordinate. Two points are most special because they are the intersection of the curve with the horizontal and vertical axes, representing V_{oc} and I_{sc}. These two parameters continue to rise with increasing tube power. The I_{sc} of GaAs is always well ahead of AlGaInP, whereas the V_{oc} is the opposite as the result of the band gap limitation. A reciprocal relationship is formed between V_{oc} and I_{sc}. P_{max} can also be obtained from the point on the *I-V* curve where the product of the horizontal and vertical coordinates is the largest. The current and voltage corresponding to P_{max} are I_{mp} and V_{mp}. P_{max} can be calculated as follows:

$$P_{max} = MAX\ (\ I \times V\ ) = I_{mp} V_{mp} \tag{1}$$

A brief judgement is made on the trend of V_{oc}, I_{sc}, and P_{max}. The *I-V* curves of GaAs and AlGaInP reveal I_{sc} shows a relatively uniform increase with the intensity of the X-rays, whereas the V_{oc} increases faster and then slower. From the rate of increase of the data it can be observed that the I_{sc} of GaAs seems to be more sensitive to the response of the intensity of the radiation field. Compared with GaAs, AlGaInP varies more smoothly in both parameters. Moreover, the variation degree of P_{max} with the intensity of the radiation field is different for GaAs and AlGaInP. The sensitivity of the three parameters of current, voltage and power output to the radiation field can be fully utilized to accurately select different photovoltaic cells and to play the effect of their radiation energy transfer applications. Photovoltaic cells are expected to fulfil the dual functions of radiant energy conversion and radiation intensity monitoring, such as self-powered monitoring devices.

Radio-luminescent mode analysis

As shown in Fig. 3, the I_{sc} of AlGaInP in both modes increases by a factor of 11.74 when the tube power rises from 30 W to 110 W. This result inspires us that I_{sc} may be an ideal parameter to reflect the intensity of radiation. The possibility that our photovoltaic cells can be used for radiation monitoring has been initially proven. After the addition of ZnS:Cu fluorescent layer, the overall increase in I_{sc} of GaAs and AlGaInP is about 13 % and 70 %.

However, the ZnS:Cu fluorescent layer may not always play a unidirectional positive role in the energy conversion process. The variation pattern of V_{oc}, *FF*, and P_{max} with X-ray tube power before and after the addition of the ZnS:Cu fluorescent layer is fascinating. An example is the undulation in V_{oc} of both photovoltaic cells before and after the addition of the ZnS:Cu fluorescent layer. The V_{oc} of AlGaInP increases slightly, whereas the drop in V_{oc} of GaAs is more pronounced as the tube power decreases. The rise and fall of P_{max} also exhibits the two-faced role of the ZnS:Cu fluorescent layer. Fig. 4 shows the P_{max} of AlGaInP in the RL mode increases by more than 70 %, whereas the P_{max} of GaAs in the RL mode is lower than that of the RV mode. At its lowest, the former is only 53.7 % of the latter. As the tube power of the X-ray rises, the disparity between RL and RV modes narrows.

FF is the bridge that establishes the link among P_{max}, I_{sc}, and V_{oc}. It is calculated as follows:

$$FF = \frac{P_{max}}{I_{sc} V_{oc}} = \frac{I_{mp} V_{mp}}{I_{sc} V_{oc}} \tag{2}$$

Thus, *FF* can also be used to measure the proximity of I_{mp} to I_{sc} and V_{mp} to V_{oc}. Fig. S3 shows the change in *FF* of GaAs is similar to that of V_{oc} after the addition of the ZnS:Cu fluorescent layer. The lower the X-ray tube power, the greater the deviation from the ideal situation compared to the RV mode. Even an increase in I_{sc} cannot eliminate the drop in P_{max} caused by this deviation. In contrast, I_{sc}, V_{oc}, and *FF* of AlGaInP all increase after the addition of the ZnS:Cu fluorescent layer. P_{max} also increases in parallel. Fluctuations in P_{max} are the result of the combined effect of I_{sc}, V_{oc}, and *FF*. According to the prediction, V_{oc} and *FF* will be saturated gradually, so the contribution of these two to P_{max} will be reduced, and then I_{sc} will dominate. This agrees with the experimental results that the two parameters of I_{sc} and P_{max} of AlGaInP are positively correlated after the addition of ZnS:Cu fluorescent layer. Therefore, the P_{max} may serve as a parameter comparable with I_{sc} in reflecting the intensity of radiation.

To verify the effect of different fluorescent materials satisfying the matching requirement on the output performance in the RL mode, the CsI scintillator was selected for testing. Figs. 5 and S4 show the output performance of GaAs and AlGaInP when coupled with the CsI scintillator. The I_{sc} and P_{max} of both photovoltaic cells are raised to a whole new level. They achieve an order of magnitude jump at a tube power of

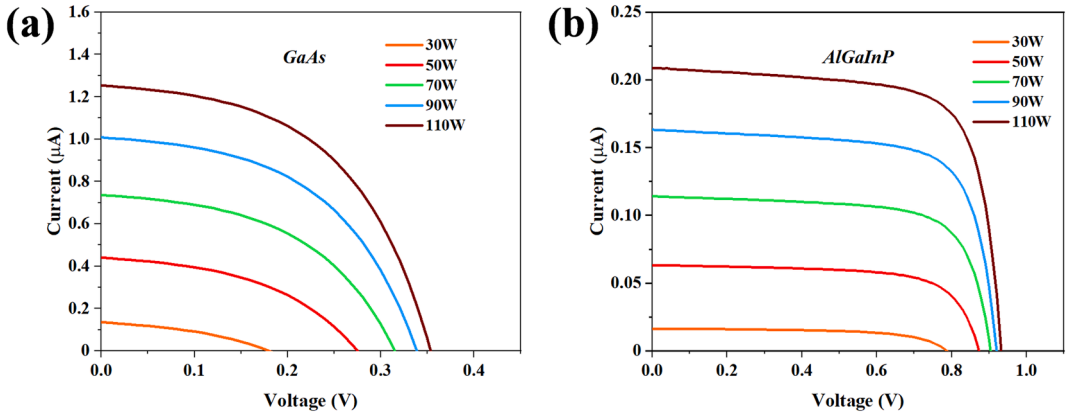

Fig. 2. *I-V* curves of two photovoltaic cells in RV mode: (a) GaAs and (b) AlGaInP.

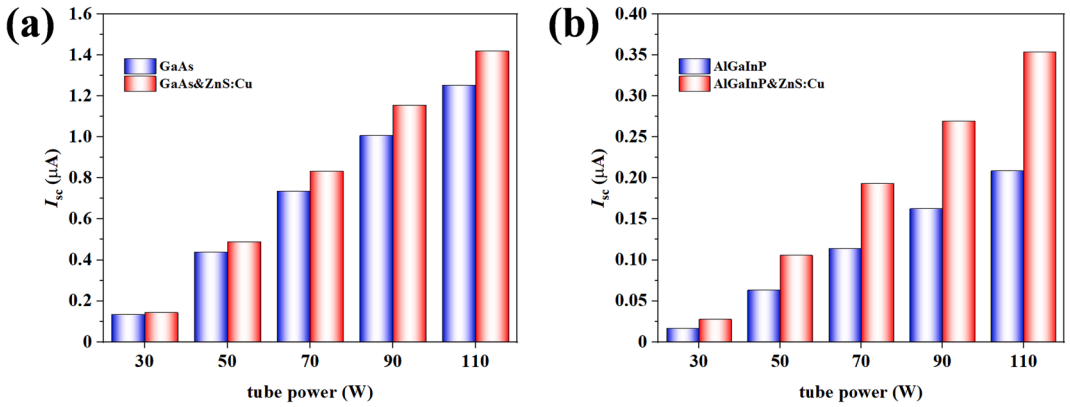

Fig. 3. I_{sc} of two photovoltaic cells in two modes: (a) GaAs and (b) AlGaInP.

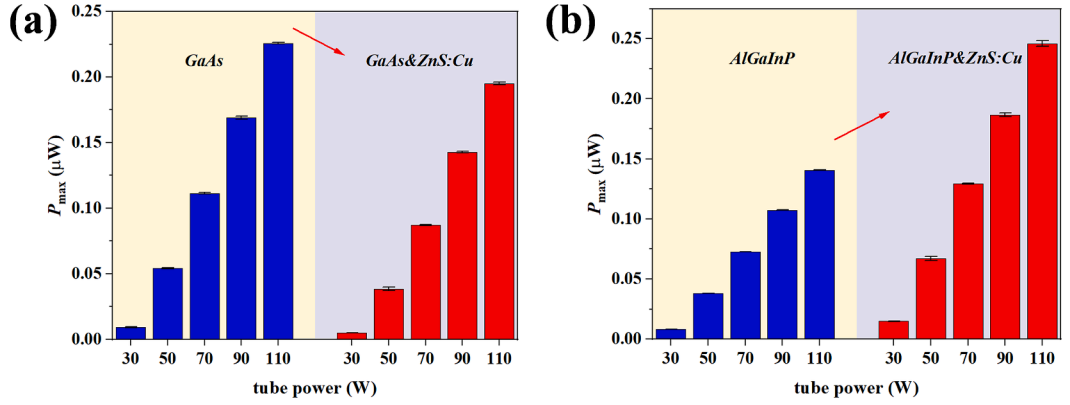

Fig. 4. P_{max} of two photovoltaic cells in two modes: (a) GaAs and (b) AlGaInP.

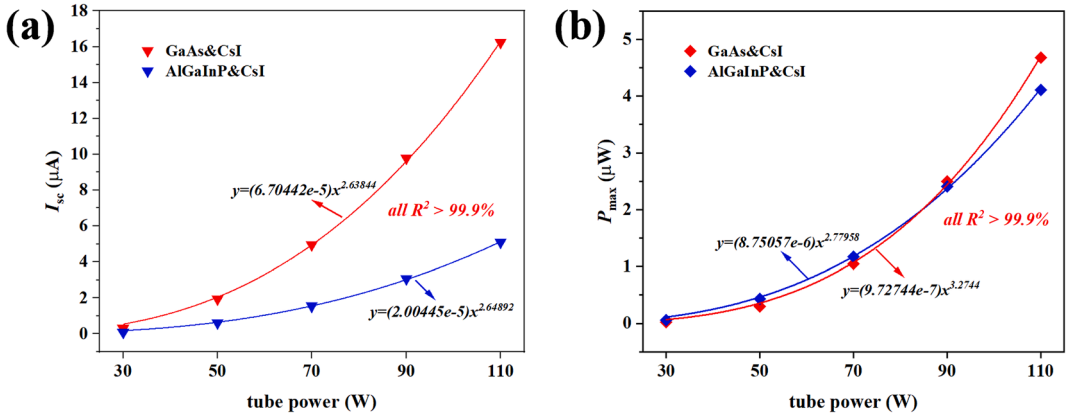

Fig. 5. (a) I_{sc} and (b) P_{max} of two photovoltaic cells in the RL mode with CsI scintillator as fluorescent material.

110 W. Tables S1 and S2 comprehensively show the comparison of I_{sc} and P_{max} of the photovoltaic cells in both modes. The use of different types of radiation energy can be achieved by the targeted selection of suitable scintillators and matching photovoltaic cells in accordance with the characteristics of each type of radiation. These results are equally informative for wireless energy transfer for other types of radiation. The exponential increase of I_{sc} and P_{max} with radiation field intensity also provides a reference for the design of micro detectors.

Output performance enhancement with stacked layer

Based on the above, the scheme of a stacked layer consisting of two fluorescent materials was further investigated. The schematic diagram of the stacked layers is shown in Fig. S5. Fig. S2 shows the transmittance of CsI scintillator increases with increasing wavelength, whereas the transmittance of the ZnS:Cu fluorescent layer increases and then decreases, eventually stabilizing at around 5.5 %. In the corresponding wavelength range of the peak emission spectrum (about 500–550 nm), the difference in transmittance between the two is more than 7 times. The main reason for setting the stacked layer is to enhance the interaction between the fluorescent material and the X-rays and to reduce the self-absorption losses of fluorescent photons due to differences in transmittance simultaneously.

Fig. 6 shows the I_{sc} and P_{max} of GaAs and AlGaInP, when they are

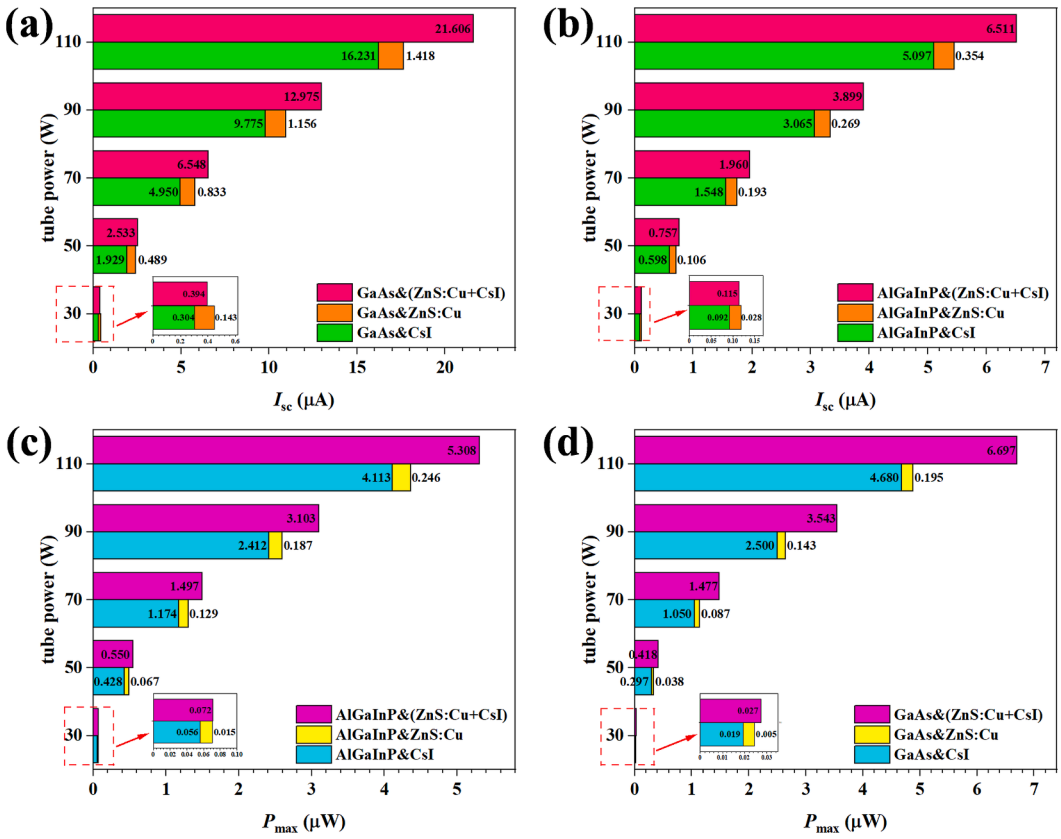

Fig. 6. I_{sc} and P_{max} of photovoltaic cells with different fluorescent material solutions: (a) I_{sc} of GaAs, (b) I_{sc} of AlGaInP, (c) P_{max} of GaAs, and (d) P_{max} of AlGaInP.

coupled with the ZnS:Cu fluorescent layer, CsI scintillator, and the stacked layer, respectively. The stacked layer once again boosts I_{sc} and P_{max}. Compared with the case with the CsI scintillator only, I_{sc} and P_{max} rise by 25 %–33 % and 28 %–43 %, respectively. It is encouraging to see that the stacked layer produces an enhancement similar to the synergistic effect. This enhancement is foreseen to be even more prominent when the radiation field increases. This result also provides a new idea for improving the output performance in RL mode.

Assessment of prospects for radiation monitoring applications

As shown in Fig. 7, I_{sc} and P_{max} show a linear relationship with tube power. The fitting degrees of all fitted curves reach more than 99 %. Tube power can be interconverted with other physical quantities that reflect the strength of the radiation field, such as dose and flux. This result validates the reasonableness of our inference that I_{sc} and P_{max} could be important parameters for monitoring intensity of the radiation field.

In terms of monitoring effectiveness, GaAs is more preferable to AlGaInP considering I_{sc}. This is a determination primarily based on the slopes of the fitted curves in Fig. 7(a). Due to the difference of band gap, the numerical difference of I_{sc} between GaAs and AlGaInP is more evident when the tube power increases. Adjusting the band gap of the photovoltaic cell is an alternative way to improve the monitoring effectiveness. However, from the point of view of P_{max}, AlGaInP coupled with the ZnS:Cu fluorescence layer is more effective. This finding suggests suitable materials play an active role in wireless energy transfer and radiation field intensity monitoring in the RL mode.

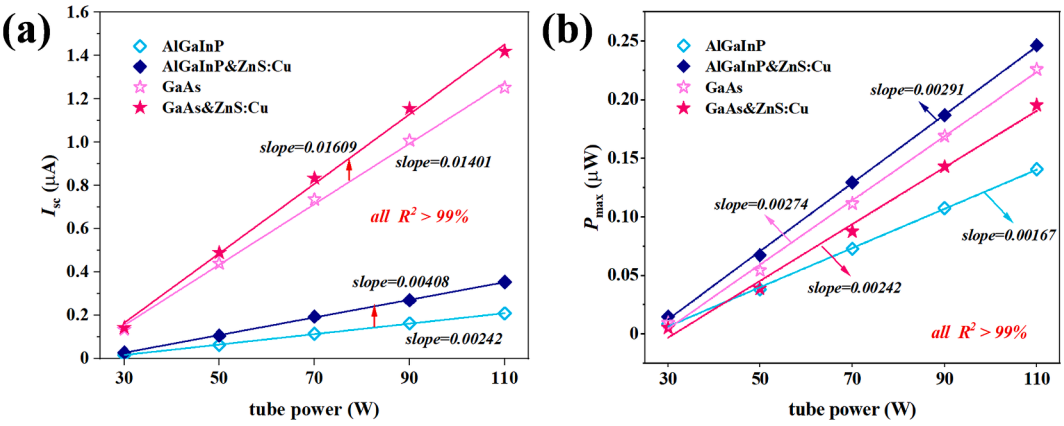

Fig. 7. (a) I_{sc} and (b) P_{max} of two photovoltaic cells as a function of tube power.

Assessment of prospects for wireless energy transfer applications

X-rays with high energy and strong penetrating ability can realize long distance propagation in the air, using this characteristic X-rays can accomplish non-contact energy transfer. The effect of distance on the effectiveness of this kind of wireless energy transfer cannot be ignored. Four AlGaInP-based energy conversion modules were tested to analyze their output performance at a distance of 10–90 cm from the exit of the X-ray tube. Fig. 8(a–b) and Figs. S6–S7 show that the coupling of AlGaInP with the stacked layer is consistently superior to three other combinations for the same distance and tube power. The advantage of the stacked layer becomes more prominent with higher tube power and equal distance. As can be seen from Fig. 8 (a-b), the increase in I_{sc} and P_{max} of AlGaInP coupled with the stacked layer can even exceed 100 % when the tube power increases from 70 W to 110 W per 20 W interval when the distance is fixed at 10 cm. When the tube power is fixed at 110 W, the I_{sc} and P_{max} of AlGaInP coupled with CsI or stacked layer are 20 times or more than the other two conversion modules. The superiority of the stack layer is again apparent. This outcome indicates that X-rays retain some intensity after a certain distance of transmission. The content of X-ray-based wireless energy transfer technology is further enriched and extended.

Fig. 8(c–d) show the decay of I_{sc} and P_{max} with distance for different combinations at a tube power of 30 W. Data for X-ray tube powers of 50–110 W are shown in Figs. S8–S9. The decreasing speed of I_{sc} and P_{max} is first fast and then slow. When the distances between AlGaInP and X-ray tube outlet increase from 10 cm to 30 cm, the decrease is the largest. Compared with I_{sc}, the attenuation trend of P_{max} is more consistent. According to the fitted curve, the attenuation law of the P_{max} with distance conforms to the following relation:

$$y = a*\exp\left(-\frac{x}{b}\right) + c \tag{3}$$

The values of a, b, and c are shown in Fig. S10. The performance attenuation of different modules is similar. Hence, the maximum distance at which X-rays can be converted is approximately the same for different modules. That the attenuation of X-rays with distance is not dependent on their intensity can be assumed. This assumption can be further borne out by the fact that the fitted relationship shown in Eq. (3) is consistent with the pattern of X-ray attenuation in air. The fitted relationship is also of great importance for the the selection of the power of the electrical devices and intensity monitoring at different locations in the radiation field. Additionally, these two aspects can be considered together, for example, installing micro-alarms of different power at different locations in the radiation field.

Conclusion

In this work, the module integrating a compact photovoltaic cell with a highly matched fluorescent material realized the dual functions of energy conversion utilization of external radiation field and intensity monitoring. A new method was proposed to characterize X-ray intensity based on the linear variation of electrical properties such as I_{sc} and P_{max} with the intensity of the radiation field. The correct selection of fluorescent materials helped to improve the effect of energy conversion and radiation monitoring. More than 20 times improvement in output performance provided by the stacked layer was quite impressive. Moreover, the feasibility of using X-rays for wireless energy transfer was verified and the maximum output power of all four energy conversion modules showed an exponential decay trend with distance. These results also provide important references for the development of wireless energy transfer technology based on X-ray and new X-ray detection methods. On this basis, a series of new semiconductor devices that respond to radiation fields can be derived, such as X/γ radiation detector and radiation sensors.

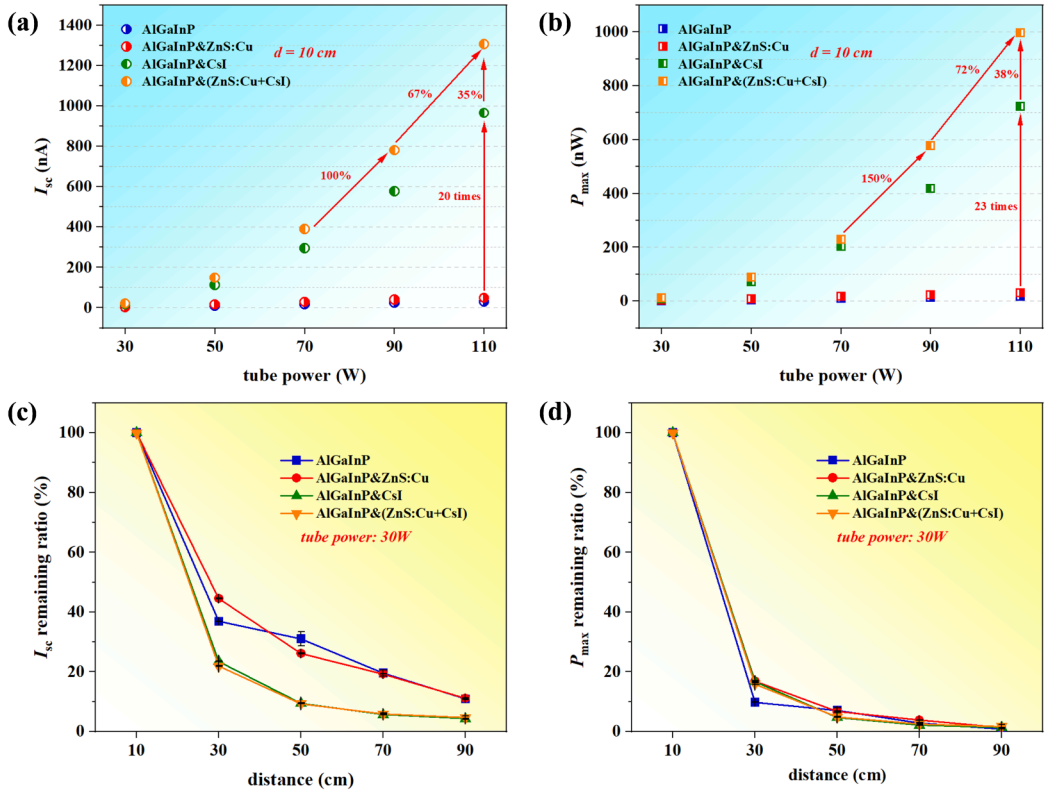

Fig. 8. (a) I_{sc} of different conversion modules when the distance is fixed, (b) P_{max} of different conversion modules when the distance is fixed, (c) attenuation of I_{sc} with distance for different conversion modules, and (d) attenuation of P_{max} with distance for different conversion modules.

CRediT authorship contribution statement

Yishui Wu: Conceptualization, Investigation, Writing – original draft. **Zhiheng Xu:** Validation, Resources, Writing – review & editing. **Yunpeng Liu:** Conceptualization, Writing – review & editing. **Tongxin Jiang:** Writing – review & editing. **Haisheng San:** Conceptualization, Writing – review & editing. **Xiaobin Tang:** Supervision.

Declaration of competing interest

The authors declare that they have no known competing financial interests or personal relationships that could have appeared to influence the work reported in this paper.

Data availability

Data will be made available on request.

Acknowledgments

We would like to thank professor Kelum A.A. Gamage (University of Glasgow) for his valuable suggestions on our work and refinement of the manuscript. This work is supported by the National Natural Science Foundation of China (Grant Nos. 12005101 and 12175190), the China Postdoctoral Science Foundation (Grant No. 2022 M711613), the Natural Science Foundation of Jiangsu Province (Grant No. BK20201288), and the Jiangsu Funding Program for Excellent Postdoctoral Talent (Grant No. 2022ZB235).

Appendix A. Supplementary data

Supplementary data to this article can be found online at https://doi.org/10.1016/j.seta.2023.103552.

References

[1] Khan MI, Asfand F, Al-Ghamdi SG. Progress in technology advancements for next generation concentrated solar power using solid particle receivers. Sustain Energy Technol Assessments 2022;54:102813. https://doi.org/10.1016/j.seta.2022.102813.
[2] Erixno O, Rahim NA, Ramadhani F, Adzman NN. Energy management of renewable energy-based combined heat and power systems: A review. Sustain Energy Technol Assessments 2022;51:101944. https://doi.org/10.1016/j.seta.2021.101944.
[3] Tang J, Ni H, Peng R, Wang N, Zuo L. A review on energy conversion using hybrid photovoltaic and thermoelectric systems. J Power Sources 2023;562:232785. https://doi.org/10.1016/j.jpowsour.2023.232785.
[4] Saravanan A, Kumar PS, Nhung TC, Ramesh B, Srinivasan S, Rangasamy G. A review on biological methodologies in municipal solid waste management and landfilling: Resource and energy recovery. Chemosphere 2022;309:136630. https://doi.org/10.1016/j.chemosphere.2022.136630.
[5] Wardhana EM, Mutsuda H, Tanaka Y, Nakashima T, Kanehira T, Maeda S, et al. Characteristics of electric performance and key factors of a hybrid piezo/triboelectric generator for wave energy harvesting. Sustain Energy Technol Assessments 2022;50:101757. https://doi.org/10.1016/J.SETA.2021.101757.
[6] Murugan G, Vijayarajan S. IoT based secured data monitoring system for renewable energy fed micro grid system. Sustain Energy Technol Assessments 2023;57:103244. https://doi.org/10.1016/j.seta.2023.103244.
[7] Zhao Y, Li X, Hou N, Yuan T, Huang S, Li L, et al. Self-powered sensor integration system based on thorn-like polyaniline composites for smart home applications. Nano Energy 2022;104:107966. https://doi.org/10.1016/j.nanoen.2022.107966.
[8] Lee B, Cho H, Park KT, Kim JS, Park M, Kim H, et al. High-performance compliant thermoelectric generators with magnetically self-assembled soft heat conductors for self-powered wearable electronics. Nat Commun 2020;11:5948. https://doi.org/10.1038/s41467-020-19756-z.
[9] Xie J, Li Y, Yang L, Sun Y, Yuan M. A review of the recent progress of stand-alone photovoltaic-battery hybrid energy systems in space and on the ground. J Energy Storage 2022;55:105735. https://doi.org/10.1016/j.est.2022.105735.
[10] Miao X, Zhang H, Wang Q, Xia Y, Sun W. Optimum design of nuclear electric propulsion spacecraft for deep space exploration. Energy Rep 2022;8:9629–41. https://doi.org/10.1016/j.egyr.2022.07.146.
[11] Zhang T, Li Y, Chen Y, Feng X, Zhu X, Chen Z, et al. Review on space energy. Appl Energy 2021;292:116896. https://doi.org/10.1016/j.apenergy.2021.116896.
[12] Cherry SR, Sorenson JA, Phelps ME. Physics in Nuclear Medicine. 4th ed. Philadelphia: W.B. Saunders; 2012.
[13] Mettler FA, Upton AC. Medical Effects of Ionizing Radiation. 3rd ed. Philadelphia: W.B. Saunders; 2008.
[14] Chang Q, Guo S, Zhang X. Radiation shielding polymer composites: Ray-interaction mechanism, structural design, manufacture and biomedical applications. Mater Des 2023;223:112253. https://doi.org/10.1016/j.matdes.2023.112253.
[15] Prelas M, Boraas M, Aguilar FDLT, Seelig JD, Tchouaso MT, Wisniewski D. Nuclear Batteries and Radioisotopes. 1st ed. Switzerland: Springer; 2016.
[16] Bower EK, Barbanel YA, Shreter YG, Bohnert GW. Polymers, Phosphors, and Voltaics for Radioisotope Microbatteries. 1st ed. Boca Raton: CRC Press; 2002.
[17] Liu Y, Guo X, Jin Z, Tang X. Temperature dependence of ^{63}Ni–Si betavoltaic microbattery. Appl Radiat Isot 2018;135:47–56. https://doi.org/10.1016/j.apradiso.2018.01.017.
[18] Liu Y, Lu J, Li X, Xu X, He R, Wang H. A 4H–SiC betavoltaic battery based on a ^{63}Ni source. Nucl Sci Tech 2018;29:168. https://doi.org/10.1007/s41365-018-0494-x.
[19] Walton R, Anthony C, Ward M, Metje N, Chapman DN. Radioisotopic battery and capacitor system for powering Wireless Sensor Networks. Sens Actuators A 2013;203:405–12. https://doi.org/10.1016/j.sna.2013.09.010.
[20] Wang B, Yang X, Chen S, Lu S, Zhao S, Qian Q, et al. Flexible perovskite scintillators and detectors for X-ray detection. iScience 2022;25:105593. https://doi.org/10.1016/j.isci.2022.105593.
[21] Ou X, Chen X, Xu X, Xie L, Chen X, Hong Z, et al. Recent Development in X-Ray Imaging Technology: Future and Challenges. Research 2021;2021. https://doi.org/10.34133/2021/9892152.
[22] Li X, Hu X, Li C, Yang W, Wang C, Chen Y, et al. Are Inorganic Lead Halide Perovskite Nanocrystals Promising Scintillators? ACS Energy Lett 2023;8:2996–3004. https://doi.org/10.1021/acsenergylett.3c00920.
[23] Hu X, Yan P, Ran P, Lu L, Leng J, Yang Y, et al. In Situ Fabrication of $Cs_3Cu_2I_5$: Tl Nanocrystal Films for High-Resolution and Ultrastable X-ray Imaging. J Phys Chem Lett 2022;13:2862–70. https://doi.org/10.1021/acs.jpclett.2c00456.
[24] Zhou Q, Ren J, Xiao J, Lei L, Liao F, Di H, et al. Highly efficient copper halide scintillators for high-performance and dynamic X-ray imaging. Nanoscale 2021;13:19894–902. https://doi.org/10.1039/D1NR03996B.
[25] Xu Z, Tang X, Liu Y, Zhang Z, Chen W, Liu K, et al. $CsPbBr_3$ Quantum Dot Films with High Luminescence Efficiency and Irradiation Stability for Radioluminescent Nuclear Battery Application. ACS Appl Mater Interfaces 2019;11:14191–21419. https://doi.org/10.1021/acsami.9b02425.
[26] Li X, Chen J, Yang D, Chen X, Geng D, Jiang L, et al. Mn^{2+} induced significant improvement and robust stability of radioluminescence in $Cs_3Cu_2I_5$ for high-performance nuclear battery. Nat Commun 2021;12:3879. https://doi.org/10.1038/s41467-021-24185-7.
[27] Zhao C, Ren J, Lei L, Liao F, Shi X, Zhou D, et al. Tenfold efficiency improvement of x-ray radioluminescent batteries basing on GAGG: Ce single crystal scintillators. Appl Phys Lett 2021;119:223901. https://doi.org/10.1063/5.0073048.
[28] Lu L, Sun M, Lu Q, Wu T, Huang B. High energy X-ray radiation sensitive scintillating materials for medical imaging, cancer diagnosis and therapy. Nano Energy 2021;79:105437. https://doi.org/10.1016/j.nanoen.2020.105437.
[29] Ummartyotin S, Infahsaeng Y. A comprehensive review on ZnS: From synthesis to an approach on solar cell. Renew Sust Energ Rev 2016;55:17–24. https://doi.org/10.1016/j.rser.2015.10.120.
[30] Jiang T, Xu Z, Meng C, Liu Y, Tang X. In-Depth Analysis of the Internal Energy Conversion of Nuclear Batteries and Radiation Degradation of Key Materials. Energy Technol 2020;8. https://doi.org/10.1002/ente.202000667.
[31] Jiang T, Xu Z, Tang X, Yuan Z, Wang H, Bian M. Comparison and study of the preparation methods for phosphor layer in nuclear battery. Int J Energy Res 2020;45:11712–20. https://doi.org/10.1002/er.5526.
[32] Xu Z, Liu Y, Zhang Z, Chen W, Yuan Z, Liu K, et al. Enhanced radioluminescent nuclear battery by optimizing structural design of the phosphor layer. Int J Energy Res 2018;42:1729–37. https://doi.org/10.1002/er.3982.